7604 *Inorg. Chem.* **2009**, *48*, 7604–7612
DOI: 10.1021/ic900564q

Inorganic Chemistry
Article

Biomimetic Model Featuring the NH Proton and Bridging Hydride Related to a Proposed Intermediate in Enzymatic H_2 Production by Fe-Only Hydrogenase

Ming-Hsi Chiang,*,† Yu-Chiao Liu,† Shu-Ting Yang,† and Gene-Hsiang Lee‡

†*Institute of Chemistry, Academia Sinica, Nankang, Taipei 115, Taiwan, and* ‡*Instrumentation Center, National Taiwan University, Taipei 106, Taiwan*

Received January 21, 2009

Iron azadithiolate phosphine-substituted complex and its protonated species featuring the NH proton and/or bridging Fe hydride, $[Fe_2(\mu\text{-}S(CH_2)_2N^nPr(H)_m(CH_2)_2S)(\mu\text{-}H)_n(CO)_4(PMe_3)_2]_2^{(2m+2n)+}$ (**1**, $m = n = 0$; $\mathbf{[1-2H^N]^{2+}}$, $m = 1$, $n = 0$; $\mathbf{[1-2H^N2H^{Fe}]^{4+}}$, $m = n = 1$), are prepared to mimic the active site of Fe-only hydrogenase. X-ray crystallographic analyses of these three complexes reveal that two diiron subunits are linked by two azadiethylenethiolate bridges to construct a dimer-of-dimer structure. ^{31}P NMR spectroscopy confirms two trimethylphosphine ligands within the diiron moiety are arranged in the apical/basal configuration, which is consistent with the solid-state structural characterization. Deprotonation of the NH proton in $\mathbf{[1-2H^N]^{2+}}$ and $\mathbf{[1-2H^N2H^{Fe}]^{4+}}$ occurs in the presence of triethanolamine (TEOA), which generates **1** and $\mathbf{[1-2H^{Fe}]^{2+}}$, respectively. Deprotonation of the Fe hydride is accomplished by addition of bistriphenylphosphineimminium chloride ([PPN]Cl). It is observed that the Fe hydride species, $\mathbf{[1-2H^{Fe}]^{2+}}$, is a kinetic product which converts to its thermodynamically stable tautomer, $\mathbf{[1-2H^N]^{2+}}$, in solution, as evidenced by IR and NMR spectroscopy. The pK_a values of the aza nitrogen and the diiron sites are estimated to be 8.9−15.9 and <8.9, respectively. $\mathbf{[1-2H^N2H^{Fe}]^{4+}}$ has been observed to evolve H_2 electrocatalytically at a mild potential (−1.42 V vs Fc/Fc^+) in CH_3CN solution. Catalysis of $\mathbf{[1-2H^N2H^{Fe}]^{4+}}$ is found to be as efficient as that of the related diiron azadithiolate complexes. In the absence of a proton source, $\mathbf{[1-2H^N2H^{Fe}]^{4+}}$ undergoes four irreversible reduction processes at −1.26, −1.42, −1.82, and −2.43 V, which are attributed to the reduction events from $\mathbf{[1-2H^N2H^{Fe}]^{4+}}$, $\mathbf{[1-2H^{Fe}]^{2+}}$, $\mathbf{[1-2H^N]^{2+}}$, and **1**, respectively, according to bulk electrolysis and voltammetry in combination of titration experiments with acids.

Introduction

Recent efforts have been paid to the structural and functional design of biomimetic models of Fe-only hydrogenases in the hope of finding a substitute for expensive platinum working electrodes used for industrial hydrogen production.[1] Fe-only hydrogenases isolated from *Desulfovibrio desulfuricans*[2] and *Clostridium pasterianum*[3] perform both metabolism and production of H_2 ($2H^+ + 2e^- \leftrightarrow H_2$) in mild reduction potentials (−100 to −500 mV) and in high efficiency (6×10^3 s^{-1}).[4] The active site, the H-cluster, is composed of a [2Fe2S] unit linked to a [4Fe4S] ferredoxin cluster via a cysteinyl thiolate on the peptide chain.[5] The primary coordination sphere of the diiron unit in addition to the S^{cys} bridge is occupied by cyanide and carbon monoxide ligands as well as an abiological dithiolate bridge ($-SCH_2XCH_2S-$). The putative central atom of the dithiolate linker is presumed to be NH[6] albeit the possibility of CH_2 or O can not be excluded.[2,7] The presence of the NH bridgehead is important because of its potential function to act as a base to either convey protons from the protein surface to the catalytic metal site in the process of enzymatic H_2 evolution or polarize hydrogen molecules in the heterolytic cleavage process of H_2 uptake.

The proposed mechanism of enzymatic H_2 production involves two protonated species: the N-protonated species and the N-protonated, Fe-hydride species where the hydride is presumably in a terminal manner, shown in Scheme 1.[8]

*To whom correspondence should be addressed. E-mail: mhchiang@chem.sinica.edu.tw.

(1) Cammack, R.; Frey, M.; Robson, R. *Hydrogen as a Fuel: Learning from Nature*; Taylor & Francis: London and New York, 2001.
(2) Nicolet, Y.; Piras, C.; Legrand, P.; Hatchikian, C. E.; Fontecilla-Camps, J. C. *Structure* **1999**, *7*, 13–23.
(3) Peters, J. W.; Lanzilotta, W. N.; Lemon, B. J.; Seefeldt, L. C. *Science* **1998**, *282*, 1853–1858.
(4) Holm, R. H.; Kennepohl, P.; Solomon, E. I. *Chem. Rev.* **1996**, *96*, 2239–2314.
(5) (a) Adams, M. W. W.; Stiefel, E. I. *Curr. Opin. Chem. Biol.* **2000**, *4*, 214–220. (b) Huynh, B. H.; Czechowski, M. H.; Kruger, H. J.; DerVartanian, D. V.; Peck, H. D., Jr.; LeGall, J. *Proc. Natl. Acad. Sci. U.S.A.* **1984**, *81*, 3728–3732.
(6) Nicolet, Y.; de Lacey, A. L.; Vernede, X.; Fernandez, V. M.; Hatchikian, E. C.; Fontecilla-Camps, J. C. *J. Am. Chem. Soc.* **2001**, *123*, 1596–1601.
(7) Pandey, A. S.; Harris, T. V.; Giles, L. J.; Peters, J. W.; Szilagyi, R. K. *J. Am. Chem. Soc.* **2008**, *130*, 4533–4540.
(8) (a) Armstrong, F. A. *Curr. Opin. Chem. Biol.* **2004**, *8*, 133–140. (b) Cheah, M. H.; Tard, C.; Borg, S. J.; Liu, X.; Ibrahim, S. K.; Pickett, C. J.; Best, S. P. *J. Am. Chem. Soc.* **2007**, *129*, 11085–11092.

Published on Web 07/14/2009

Protonation of the iron propanedithiolate complexes and their derivatives to form the Fe(μ-H)Fe products has been well studied.[9−15] Recently the transient terminal hydride intermediates have been spectroscopically characterized.[16] On the other hand, isolation of the protonated species of the azadithiolate analogues encounters difficulties. The presence of the protonated derivatives in the reaction solution has been evidenced by NMR and FTIR spectroscopy.[17−19] The first structural report available is on $[\{(\mu\text{-}SCH_2)_2N(H)\text{-}(CH_2C_6H_4\text{-}o\text{-}Br)\}Fe_2(CO)_6]^+$ by Sun et al. In this molecule the NH proton is stabilized because of the intramolecular interaction initiated by Br of the *o*-bromobenzyl group.[20] One can speculate that hydrogen bonding within the molecule might prohibit proton relay to the catalytic Fe center from the aza nitrogen site via the agostic interaction. The only example close to the NH-FeH intermediate is the pdt derivative featuring the bridging hydride and *N*-protonated diphosphine chelate, which is recently published by the same group.[12] Unfortunately, no structural evidence of the iron thiolate phosphine derivatives possessing the azadithiolate NH proton and bridging iron hydride has been reported yet.

To elucidate the importance of the aza nitrogen site and its role in the mechanism of enzymatic H_2 production, we designed a series of iron complexes bearing azadiethylenethiolate ligands. Herein, we report the isolation and characterization of three unprecedented iron azadithiolate complexes, $[Fe_2(\mu\text{-}S(CH_2)_2N(H)^nPr(CH_2)_2S)(CO)_4(PMe_3)_2]_2\text{-}(BF_4)_2$, $\mathbf{[1-2H^N]^{2+}}$, featuring non-supported NH protons,

Scheme 1. Possible Intermediates in the Mechanism of Enzymatic H_2 Production by Fe-Only Hydrogenases

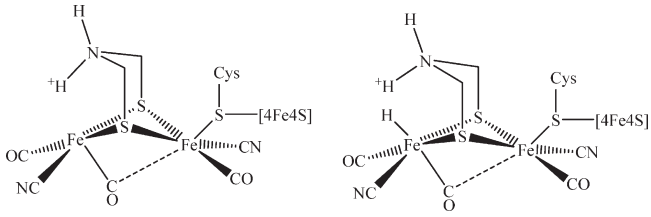

$[Fe_2(\mu\text{-}H)(\mu\text{-}S(CH_2)_2N(H)^nPr(CH_2)_2S)(CO)_4(PMe_3)_2]_2(BF_4)_4$, $\mathbf{[1-2H^N2H^{Fe}]^{4+}}$, featuring both non-supported NH protons and bridging iron hydrides, and their parent molecule, $[Fe_2(\mu\text{-}S(CH_2)_2N^nPr(CH_2)_2S)(CO)_4(PMe_3)_2]_2$, **1**. Electrocatalytic study of the NH-FeH complex shows it catalyzes reduction of protons at a mild potential in the presence of an acid.

Results and Discussion

Synthesis and Characterization of $[Fe_2(\mu\text{-}S(CH_2)_2N^nPr(CH_2)_2S)(CO)_6]_2$, 1, $[1-2H^N]^{2+}$, and $[1-2H^N2H^{Fe}]^{4+}$. Reaction of $^nPrN(CH_2CH_2SH)_2$ with triiron dodecacarbonyl in tetrahydrofuran (THF) at refluxing temperature afforded a brown red solution that contained $Fe(CO)_5$ and an orange-red product with the general formula $Fe_2(\mu\text{-}SR)_2(CO)_6$ on the basis of carbonyl vibrational frequency.[21] $Fe(CO)_5$ was removed under reduced pressure, and the resultant orange-red semi-oil was subject to column chromatography. $[Fe_2(\mu\text{-}S(CH_2)_2N^nPr(CH_2)_2S)\text{-}(CO)_6]_2$, which possesses three IR bands at 2069 (m), 2037 (vs), and 1990 (s) cm^{-1}, was obtained as a red solid. Broadness of the lowest-energy band reveals a combination of more than one peak close in energy, which is well resolved to two bands at 1999 (s) and 1988 (s) cm^{-1} in a less polar solvent such as hexane.

Reaction of $[Fe_2(\mu\text{-}S(CH_2)_2N^nPr(CH_2)_2S)(CO)_6]_2$ with PMe_3 readily affords its trimethylphosphine derivative at room temperature, $[Fe_2(\mu\text{-}S(CH_2)_2N^nPr(CH_2)_2S)(CO)_4\text{-}(PMe_3)_2]_2$, **1**. Four CO bands are identified for **1** at 1975, 1939, 1905, and 1887 cm^{-1}, which is a typical IR characteristic of the disubstituted $Fe_2(\mu$-dithiolate$)(CO)_4L_2$ complexes. The phosphine ligands are fluxional in solution as evidenced by ^{31}P NMR spectroscopy. One broad peak at 20.3 ppm is observed. This fluxional behavior is suppressed at 218 K in which two sharp bands at 13.3 and 32.6 ppm are recorded. Appearance of two ^{31}P bands indicates that these phosphine groups reside at the apical and basal positions in two different iron centers at low temperature, which is consistent with X-ray crystallographic analysis. The molecular structure of **1**, which is displayed in Figure 1, reveals that two identical diiron units are linked by two azadithiolate bridges to construct a dimer-of-dimer structure.

Formation of $\mathbf{[1-2H^N]^{2+}}$ from reaction of **1** with 2 equiv of HBF_4 is confirmed by the IR spectra in CH_3CN. The IR spectral pattern, displayed in Figure 2, remains unchanged but ν(CO) shows a shift of 10 cm^{-1} toward higher energy from **1** to $\mathbf{[1-2H^N]^{2+}}$, which is characteristic of the presence of the protonated aza nitrogen.[18,20] The NH proton is characterized as a broadband at

(9) Zhao, X.; Georgakaki, I. P.; Miller, M. L.; Mejia-Rodriguez, R.; Chiang, C.-Y.; Darensbourg, M. Y. *Inorg. Chem.* **2002**, *41*, 3917–3928.
(10) Zhao, X.; Georgakaki, I. P.; Miller, M. L.; Yarbrough, J. C.; Darensbourg, M. Y. *J. Am. Chem. Soc.* **2001**, *123*, 9710–9711.
(11) (a) Gloaguen, F.; Lawrence, J. D.; Rauchfuss, T. B.; Benard, M.; Rohmer, M.-M. *Inorg. Chem.* **2002**, *41*, 6573–6582. (b) Morvan, D.; Capon, J.-F.; Gloaguen, F.; Le Goff, A.; Marchivie, M.; Michaud, F.; Schollhammer, P.; Talarmin, J.; Yaouanc, J.-J.; Pichon, R.; Kervarec, N. *Organometallics* **2007**, *26*, 2042–2052. (c) Dong, W.; Wang, M.; Liu, X.; Jin, K.; Li, G.; Wang, F.; Sun, L. *Chem. Commun.* **2006**, 305–307. (d) Thomas, C. M.; Rüdiger, O.; Liu, T.; Carson, C. E.; Hall, M. B.; Darensbourg, M. Y. *Organometallics* **2007**, *26*, 3976–3984. (e) Dong, W.; Wang, M.; Liu, T.; Liu, X.; Jin, K.; Sun, L. *J. Inorg. Biochem.* **2007**, *101*, 506–513. (f) Zhao, X.; Chiang, C.-Y.; Miller, M. L.; Rampersad, M. V.; Darensbourg, M. Y. *J. Am. Chem. Soc.* **2003**, *125*, 518–524. (g) Xu, F.; Tard, C.; Wang, X.; Ibrahim, S. K.; Hughes, D. L.; Zhong, W.; Zeng, X.; Luo, Q.; Liu, X.; Pickett, C. J. *Chem. Commun.* **2008**, 606–608. (h) Heiden, Z. M.; Zampella, G.; De Gioia, L.; Rauchfuss, T. B. *Angew. Chem., Int. Ed.* **2008**, *47*, 9756–9759. (i) Mejia-Rodriguez, R.; Chong, D.; Reibenspies, J. H.; Soriaga, M. P.; Darensbourg, M. Y. *J. Am. Chem. Soc.* **2004**, *126*, 12004–12014. (j) Gloaguen, F.; Lawrence, J. D.; Rauchfuss, T. B. *J. Am. Chem. Soc.* **2001**, *123*, 9476–9477.
(12) Wang, N.; Wang, M.; Zhang, T.; Li, P.; Liu, J.; Sun, L. *Chem. Commun.* **2008**, 5800–5802.
(13) Ezzaher, S.; Capon, J.-F.; Gloaguen, F.; Pétillon, F. Y.; Schollhammer, P.; Talarmin, J.; Kervarec, N. *Inorg. Chem.* **2009**, *48*, 2–4.
(14) Orain, P.-Y.; Capon, J.-F.; Kervarec, N.; Gloaguen, F.; Pétillon, F.; Pichon, R.; Schollhammer, P.; Talarmin, J. *Dalton Trans.* **2007**, 3754–3756.
(15) Li, P.; Wang, M.; Chen, L.; Liu, J.; Zhao, Z.; Sun, L. *Dalton Trans.* **2009**, 1919–1926.
(16) (a) Barton, B. E.; Rauchfuss, T. B. *Inorg. Chem.* **2008**, *47*, 2261–2263. (b) Ezzaher, S.; Capon, J.-F.; Gloaguen, F.; Pétillon, F. Y.; Schollhammer, P.; Talarmin, J.; Pichon, R.; Kervarec, N. *Inorg. Chem.* **2007**, *46*, 3426–3428. (c) van der Vlugt, J. I.; Rauchfuss, T. B.; Whaley, C. M.; Wilson, S. R. *J. Am. Chem. Soc.* **2005**, *127*, 16012–16013. (d) Barton, B. E.; Olsen, M. T.; Rauchfuss, T. B. *J. Am. Chem. Soc.* **2008**, *130*, 16834–16835.
(17) Eilers, G.; Schwartz, L.; Stein, M.; Zampella, G.; De Gioia, L.; Ott, S.; Lomoth, R. *Chem.—Eur. J.* **2007**, *13*, 7075–7084.
(18) Schwartz, L.; Eilers, G.; Eriksson, L.; Gogoll, A.; Lomoth, R.; Ott, S. *Chem. Commun.* **2006**, 520–522.
(19) (a) Jiang, S.; Liu, J.; Shi, Y.; Wang, Z.; Åkermark, B.; Sun, L. *Dalton Trans.* **2007**, 896–902. (b) Wang, F.; Wang, M.; Liu, X.; Jin, K.; Dong, W.; Sun, L. *Dalton Trans.* **2007**, 3812–3819.
(20) Wang, F.; Wang, M.; Liu, X.; Jin, K.; Dong, W.; Li, G.; Åkermark, B.; Sun, L. *Chem. Commun.* **2005**, 3221–3223.
(21) King, R. B. *J. Am. Chem. Soc.* **1962**, *84*, 2460.

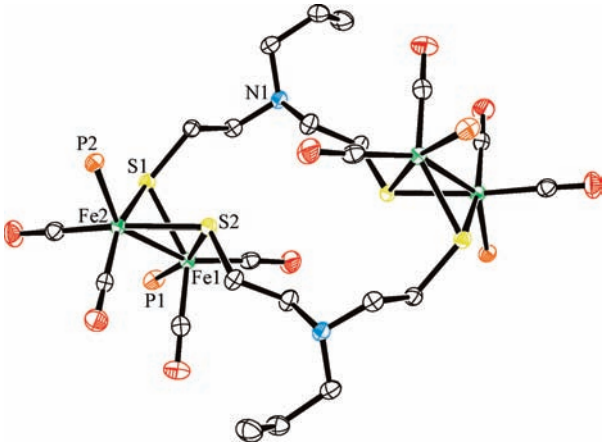

Figure 1. Molecular structure of $[Fe_2(\mu\text{-}S(CH_2)_2N^nPr(CH_2)_2S)(CO)_4(PMe_3)_2]_2$, **1**, thermal ellipsoids drawn at 50% probability level. All hydrogen atoms and methyl groups of PMe_3 are omitted for clarity.

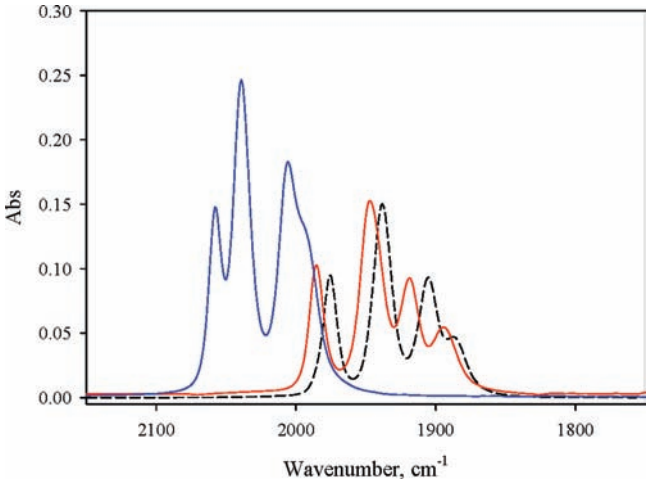

Figure 2. FTIR spectra of **1** in CH_2Cl_2 (in short dash), $[\mathbf{1-2H^N}]^{2+}$ in CH_3CN (in red), and $[\mathbf{1-2H^N2H^{Fe}}]^{4+}$ in CH_3CN (in blue).

7.42 ppm at room temperature. Two proton signals for the trimethylphosphine ligands are observed at 1.50 and 1.64 ppm with the doublet pattern because of their coupling to the phosphorus atom. Two ^{31}P NMR resonances are recorded at 10.71 and 29.43 ppm, shown in Figure 3, and are assigned to two PMe_3 groups located at the apical and basal positions, respectively.[9]

$[\mathbf{1-2H^N2H^{Fe}}]^{4+}$ is generated from the CH_3CN solution of $[\mathbf{1-2H^N}]^{2+}$ in the presence of excess HBF_4. The formation of the Fe(μ-H)Fe species because of insertion of a proton into the Fe−Fe vector is evidenced by shifts of the IR peaks to higher energy by about 90 cm^{-1}. In contrast to a minor difference corresponding to protonation of the aza nitrogen, which causes insignificant influence on the electron density about the Fe centers, such dramatic change on the IR energy, shown in Figure 2, reflects that the oxidation state of both Fe centers has altered from the original +1 state to +2 upon formation of the bridging iron hydride unit.[9,10,14] The bridging hydride is identified at −15.46 ppm in ^1H NMR spectroscopy, displayed in Figure 3. $^2J_{HP}$ values for the cis position of the hydride and phosphine are in the range of 19−24 Hz. Small J values of 3−5 Hz are characterized for the trans orientation.[9] The doublet pattern of the

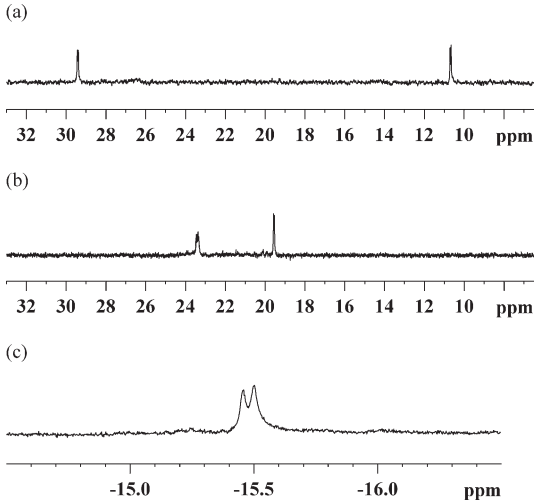

Figure 3. ^{31}P NMR spectra of (a) $[\mathbf{1-2H^N}]^{2+}$ in CD_2Cl_2, (b) $[\mathbf{1-2H^N2H^{Fe}}]^{4+}$ in CD_2Cl_2, and (c) High-field ^1H NMR spectrum of $[\mathbf{1-2H^N2H^{Fe}}]^{4+}$ in CD_2Cl_2.

hydride resonance of $[\mathbf{1-2H^N2H^{Fe}}]^{4+}$, featuring a $^2J_{HP}$ constant of 21.5 Hz, indicates that two PMe_3 groups in each Fe_2 subunit, which have the ^{31}P NMR resonances located at 19.58 and 23.43 ppm, are arranged in the apical/basal configuration. The ^{31}P NMR assignments for both $[\mathbf{1-2H^N}]^{2+}$ and $[\mathbf{1-2H^N2H^{Fe}}]^{4+}$ are consistent with their solid-state structures analyzed by single-crystal X-ray crystallography. Figure 4 shows that the PMe_3 ligands coordinate to apical and basal positions per iron of a dimer, and the Fe···Fe distance of each dimer is 2.55 and 2.58 Å for $[\mathbf{1-2H^N}]^{2+}$ and $[\mathbf{1-2H^N2H^{Fe}}]^{4+}$, respectively. The Fe···Fe distance of $[\mathbf{1-2H^N2H^{Fe}}]^{4+}$ is comparable with the metric parameters previously reported in the Fe hydride complexes, $[Fe_2(\mu\text{-H})(\mu\text{-SS})(CO)_4(P)_2]^+$ (SS = dithiolate linkers; P = phosphines).[9,10]

Deprotonation and Tautomerization. Triethanolamine (TEOA, pK_a^{TEOA} = 15.9 in CH_3CN)[22] is an effective agent to remove protons of the quaternary ammonium cations.[15,18] It was found that **1** was quantitatively recovered from reaction of $[\mathbf{1-2H^N}]^{2+}$ with TEOA. The same deprotonation process can be observed for $[\mathbf{1-2H^N2H^{Fe}}]^{4+}$ in the presence of 2 equiv TEOA. A new IR spectrum with the similar peak pattern with that of $[\mathbf{1-2H^N2H^{Fe}}]^{4+}$ emerged in the lower energy region. This approximate 10 cm^{-1} shift is comparable with the results observed for the adt diiron analogues with respect to their adt diiron NH species.[17,18] The new species is assigned to $[\mathbf{1-2H^{Fe}}]^{2+}$. It is discovered that $[\mathbf{1-2H^{Fe}}]^{2+}$ is not a stable species which converts to its tautomer, $[\mathbf{1-2H^N}]^{2+}$, in solution over time, as indicated by the infrared spectra (Figure 5). This observation is in contrast to the results of the adt diiron complexes in which the FeH species is presumably more stable than its NH counterpart.[17] Rauchfuss et al. has discovered that $[Fe_2((\mu\text{-}SCHMe)_2NH_2)(CO)_4(PMe_3)_2]^+$ slowly tautomerizes to its bridging hydride isomer, $[Fe_2((\mu\text{-}SCHMe)_2NH)(\mu\text{-H})(CO)_4(PMe_3)_2]^+$, in CH_3CN solution.[23] Proton transfer

(22) Izutsu, K. *Acid-Base Dissociation Constants in Dipolar Aprotic Solvents*; Blackwell: Oxford, U.K., 1990.
(23) Stanley, J. L.; Heiden, Z. M.; Rauchfuss, T. B.; Wilson, S. R.; De Gioia, L.; Zampella, G. *Organometallics* **2008**, *27*, 119–125.

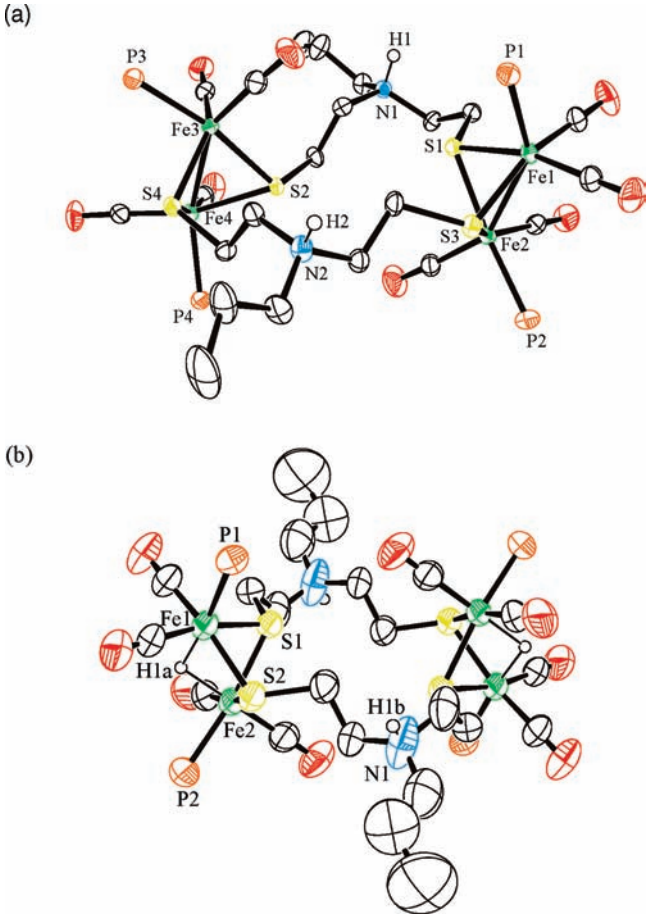

Figure 4. Molecular structures of (a) $[Fe_2(\mu\text{-}S(CH_2)_2N^nPr(H)(CH_2)_2S)(CO)_4(PMe_3)_2]_2^{2+}$, $\mathbf{[1-2H^N]^{2+}}$, thermal ellipsoids drawn at 50% probability level. (b) $[Fe_2(\mu\text{-}H)(\mu\text{-}S(CH_2)_2N^nPr(H)(CH_2)_2S)(CO)_4(PMe_3)_2]_2^{4+}$, $\mathbf{[1-2H^N2H^{Fe}]^{4+}}$, thermal ellipsoids drawn at 20% probability level. All hydrogen except NH hydrogen and bridging hydride atoms are omitted for clarity. All methyl groups of PMe_3 are also omitted for clarity.

from the pendant nitrogen site in $[Fe_2(\mu\text{-pdt})(\kappa^2\text{-}(Ph_2PCH_2)_2N(H)CH_3)(CO)_4]^+$ to the Fe center was recently observed by Talarmin et al.[13] To confirm $[1-\mathbf{2H^N}]^{2+}$ being the thermodynamically stable product, prolonged stirring was applied to the solution containing $\mathbf{[1-2H^N]^{2+}}$. No spectral change for formation of $\mathbf{[1-2H^{Fe}]^{2+}}$ was witnessed. When excess TEOA was added to the solution of $\mathbf{[1-2H^N2H^{Fe}]^{4+}}$, both of $\mathbf{[1-2H^{Fe}]^{2+}}$ and **1** were formed immediately and eventually the latter is the final product present in the solution. It is rationalized that **1** is formed owing to instant deprotonation of $\mathbf{[1-2H^N]^{2+}}$ which is generated via the tautomerization process from $\mathbf{[1-2H^{Fe}]^{2+}}$.

Deprotonation of the iron hydride is accomplished by addition of Cl^- ($pK_a^{HCl} \approx 8.9$ in CH_3CN),[22] as previously reported.[18,24] Addition of 2 equiv of [PPN]Cl promotes the dehydride reaction of $\mathbf{[1-2H^N2H^{Fe}]^{4+}}$ and $\mathbf{[1-2H^{Fe}]^{2+}}$ to generate $\mathbf{[1-2H^N]^{2+}}$ and **1**, respectively. The pK_a values of the aza nitrogen ($8.9 < pK_a^N < 15.9$) and the diiron sites ($pK_a^{FeFe} < 8.9$) are then estimated from studies of protonation and deprotonation. The reaction scheme involving the protonation, deprotonation, and tautomerization processes of **1** and its protonated species is depicted in Scheme 2.

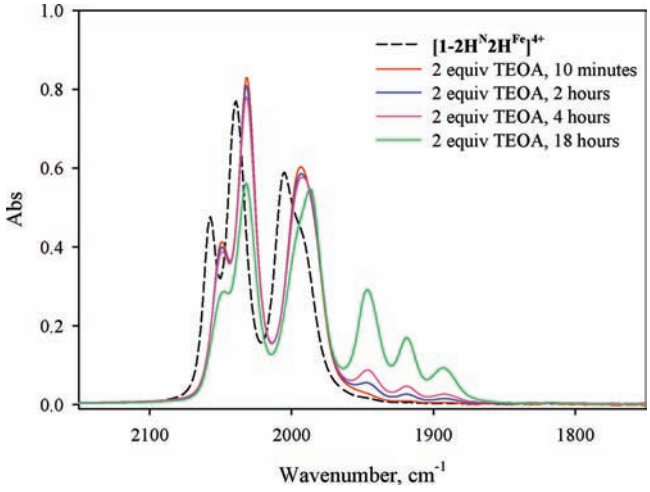

Figure 5. FTIR spectral changes for $\mathbf{[1-2H^N2H^{Fe}]^{4+}}$ upon deprotonation by TEOA in CH_3CN.

Electrochemistry of $\mathbf{[1-2H^N2H^{Fe}]^{4+}}$ in the Presence of HBF_4. Electrocatalytic activity of $\mathbf{[1-2H^N2H^{Fe}]^{4+}}$ was monitored in CH_3CN solution under N_2 with stepwise addition of HBF_4, shown in Figure 6. In the absence of a proton source, $\mathbf{[1-2H^N2H^{Fe}]^{4+}}$ undergoes four irreversible reduction processes at −1.26, −1.42, −1.82, and −2.43 V (vs Fc/Fc^+). The redox wave at the potential of −1.26 V is attributed to reduction of $\mathbf{[1-2H^N2H^{Fe}]^{4+}}$ from $Fe^{II}Fe^{II}$ to $Fe^{I}Fe^{II}$. According to bulk electrolysis at −1.34 V (vide infra), the subsequent reduction event at -1.42 V is assigned to the reduction pair ($Fe^{II}Fe^{II}$/$Fe^{I}Fe^{II}$) of $\mathbf{[1-2H^{Fe}]^{2+}}$.[12,17] The second reduction peak shows a tremendous increase of its current intensity, but the remainder of the cyclic voltammograms does not appear to show any significant influence when the acid is added into the electrochemical cell. Such enhancement of the peak current for the reduction process at −1.42 V, which shows the linear relationship with sequential increments of acid added, is consistent with electrocatalytic H_2 formation at this potential.[25]

A new reduction wave at −1.73 V is observed only when HBF_4 is present. Its current intensity also increases linearly with the acid concentration. When its peak current was plotted against equivalents of acid added, a linear dependence (slope = 7.7×10^{-5}) was obtained. This steeper slope compared with that (slope = 6.1×10^{-5}) for the reduction wave at −1.42 V, shown in Figure 7, and the appearance of the second catalytic event specific in the presence of more acids indicate that protonation of the reduced species in acidic solution occurs, and the rate of this second electrocatalytic process of proton reduction is faster than the initial one. Analysis of gas evolved from both electrochemical processes by gas chromatography confirms hydrogen to be the sole content in the gaseous product.

(24) Zhao, X.; Hsiao, Y.-M.; Lai, C.-H.; Reibenspies, J. H.; Darensbourg, M. Y. *Inorg. Chem.* **2002**, *41*, 699–708.

(25) (a) Bhugun, I.; Lexa, D.; Savéant, J.-M. *J. Am. Chem. Soc.* **1996**, *118*, 3982–3983. (b) Felton, G. A. N.; Vannucci, A. K.; Chen, J.; Lockett, L. T.; Okumura, N.; Petro, B. J.; Zakai, U. I.; Evans, D. H.; Glass, R. S.; Lichtenberger, D. L. *J. Am. Chem. Soc.* **2007**, *129*, 12521–12530. (c) Capon, J.-F.; Ezzaher, S.; Gloaguen, F.; Pétillon, F. Y.; Schollhammer, P.; Talarmin, J. *Chem.—Eur. J.* **2008**, *14*, 1954–1964. (d) Borg, S. J.; Behrsing, T.; Best, S. P.; Razavet, M.; Liu, X.; Pickett, C. J. *J. Am. Chem. Soc.* **2004**, *126*, 16988–16999.

Scheme 2. Reactions Scheme for Protonation of **1**, Deprotonation of $[\mathbf{1-2H^N}]^{2+}$, $[\mathbf{1-2H^{Fe}}]^{2+}$, and $[\mathbf{1-2H^N2H^{Fe}}]^{4+}$, and Tautomerization of $[\mathbf{1-2H^{Fe}}]^{2+}$ to $[\mathbf{1-2H^N}]^{2+}$

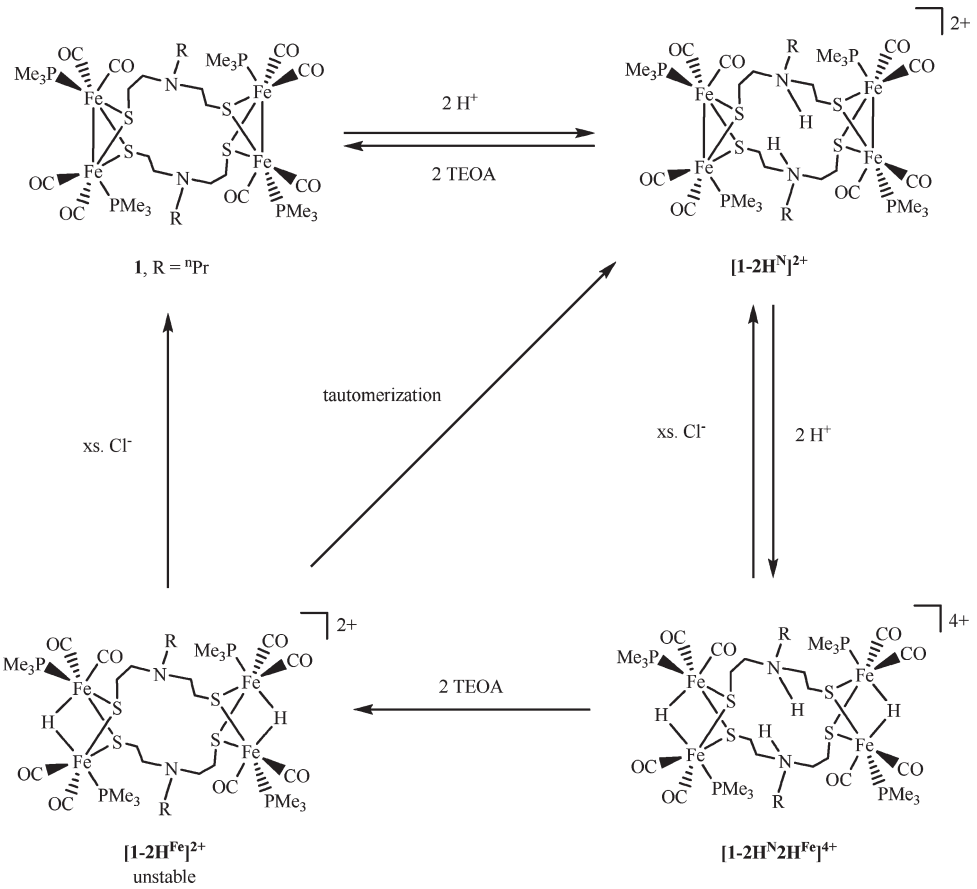

Controlled-potential electrolysis of $[\mathbf{1-2H^N2H^{Fe}}]^{4+}$ performed in CH_3CN solution at -1.34 V in the absence of acid was monitored by in situ infrared spectroscopy in a custom-made airtight cell under N_2. H_2 evolution is visible on the surface of the working electrode during electrolysis, which causes erratic spikes in the current−potential plot. The intensity of the initial IR peaks from $[\mathbf{1-2H^N2H^{Fe}}]^{4+}$ decreases, and the ν(CO) bands of $[\mathbf{1-2H^{Fe}}]^{2+}$ emerge at the lower energy (2049, 2032, and 1993 cm^{-1}). Figure 8 displays the IR changes from $[\mathbf{1-2H^N2H^{Fe}}]^{4+}$ to $[\mathbf{1-2H^{Fe}}]^{2+}$ in which the isosbestic behavior is observed, indicative of the absence of intermediates.[26] $[\mathbf{1-2H^{Fe}}]^{2+}$ subsequently transforms to $[\mathbf{1-2H^N}]^{2+}$ in solution as evidenced by growth of its IR signature bands at 1982, 1945, 1914, and 1892 cm^{-1}.

Assignment of the two reduction waves at the most negative potential is made possible by titration experiments of **1** with HOTf and HBF_4, respectively, monitored by FTIR spectroscopy and cyclic voltammetry. Figure 9 shows results from the HOTf reaction. A new irreversible peak appearing at -1.82 V in addition to the initial reduction wave at -2.43 V corresponding to the $\mathbf{1}^{2-}/\mathbf{1}$ pair is confirmed by IR to be the reduction of the protonated species, $[\mathbf{1-2H^N}]^{2+}$, when 2 equiv of HOTf is added to the CH_3CN solution of **1**. This 600 mV shift toward more positive potential is consistent with the introduction of protons to the aza nitrogen sites of **1**. The result is compared with an independent voltammogram of $[\mathbf{1-2H^N}]^{2+}$ recorded in CH_3CN solution, confirming the observation of two irreversible processes at the identical potentials. With increasing acid concentration, the redox behavior of the solution reveals the similarity to that of $[\mathbf{1-2H^N2H^{Fe}}]^{4+}$ in the presence of acid. The FTIR spectra indicate that $[\mathbf{1-2H^N}]^{2+}$ is generated initially and then its amount decreases with increase of $[\mathbf{1-2H^N2H^{Fe}}]^{4+}$ which eventually is the sole product in the acidic solution.

Our results point to two electrocatalytic routes to H_2 production from the complex $[\mathbf{1-2H^N2H^{Fe}}]^{4+}$. Current intensity of process I reaches a plateau when acid concentration is about 4 equiv. This suggests that reduction of the catalyst at the electrode has the same rate as its oxidation by the acid under such condition.[27] Catalytic activity of $[\mathbf{1-2H^N2H^{Fe}}]^{4+}$ can be compared with that of the related adt diiron complexes if its proton reduction mechanism involved with process I is presumably similar with that supported by the adt diphosphine species since a close catalytic environment including an aza nitrogen and two phosphine sites is present within each diiron unit. The peak current of process I is found to level off at about 340 μA, which refers to 170 μA for each Fe_2 subset in 1 mM of

(26) Olsen, M. T.; Bruschi, M.; De Gioia, L.; Rauchfuss, T. B.; Wilson, S. R. *J. Am. Chem. Soc.* **2008**, *130*, 12021–12030.

(27) (a) Bard, A. J.; Faulkner, L. R. *Electrochemical Methods: Fundamentals and Applications*; John Wiley & Sons: New York, 1980. (b) Andrieux, C. P.; Blocman, C.; Dumas-Bouchiat, J. M.; M′Halla, F.; Savéant, J. M. *J. Electroanal. Chem.* **1980**, *113*, 19–40.

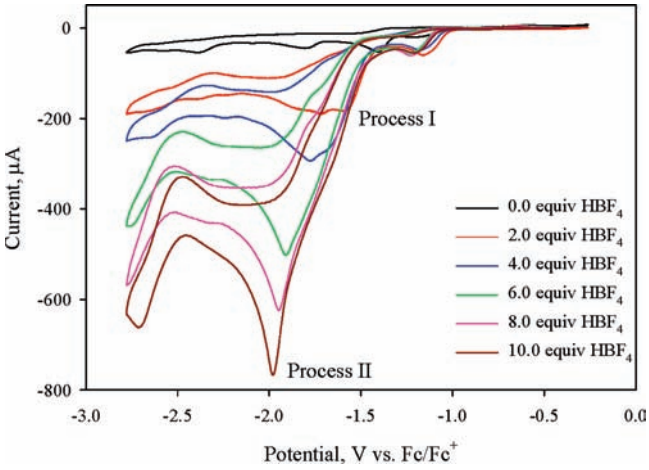

Figure 6. Cyclic voltammograms of $[\mathbf{1}{-}\mathbf{2H^N2H^{Fe}}]^{4+}$ (1 mM) with HBF_4 in CH_3CN (ν = 100 mV s^{-1}, potentials are versus Fc/Fc^+).

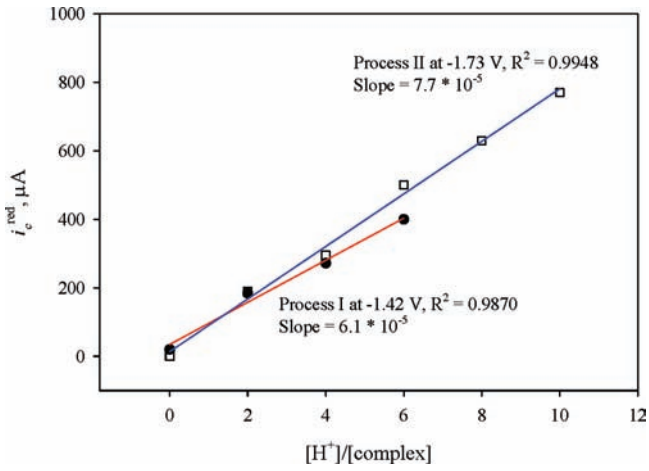

Figure 7. Dependence of current (i_c^{red}) vs equivalents of HBF_4 added for $[\mathbf{1}{-}\mathbf{2H^N2H^{Fe}}]^{4+}$ (at RT, 1 mM in CH_3CN), where i_c^{red} is peak catalytic current.

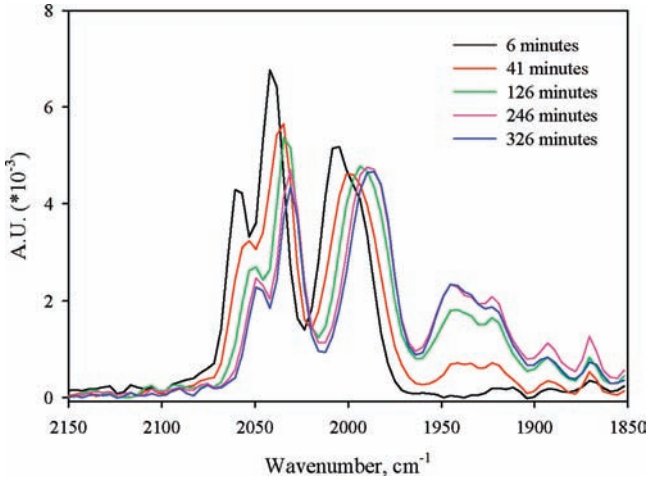

Figure 8. Spectral changes monitored by in-situ IR spectroscopy over time for $[\mathbf{1}{-}\mathbf{2H^N2H^{Fe}}]^{4+}$ upon electrolysis at −1.35 V in CH_3CN.

$[\mathbf{1}{-}\mathbf{2H^N2H^{Fe}}]^{4+}$. This value is comparable to 150 μA observed for $[Fe_2(\mu\text{-}SCH_2N(^iPr)CH_2S)(CO)_4(\kappa^2\text{-}dppe)]$.[28]

(28) Ezzaher, S.; Orain, P.-Y.; Capon, J.-F.; Gloaguen, F.; Pétillon, F. Y.; Roisnel, T.; Schollhammer, P.; Talarmin, J. *Chem. Commun.* **2008**, 2547–2549.

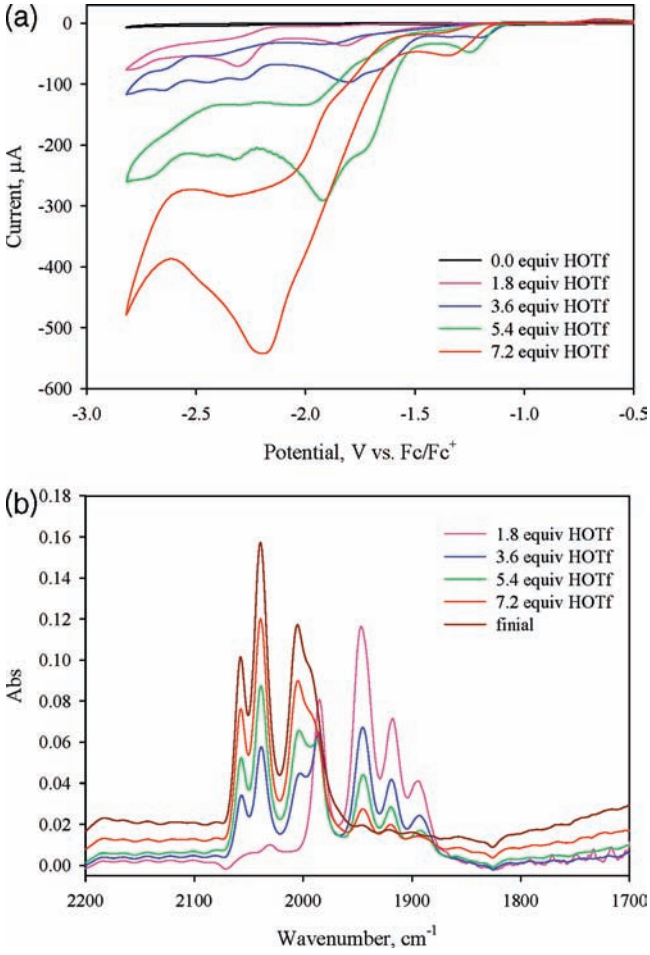

Figure 9. Cyclic voltammograms of titration of **1** (1 mM in CH_3CN) by HOTf and their corresponding FTIR spectra.

The catalytic rate of both model complexes is thus estimated to be the same. In other words, structural discrepancy of $[\mathbf{1}{-}\mathbf{2H^N2H^{Fe}}]^{4+}$ from $[Fe_2(\mu\text{-adt})(CO)_4(P)_2]$ (P = phosphine ligand) does not affect its ability to electrocatalyze the formation of H_2.

Conclusions

This report presents the characterization of the biomimetic iron thiolate complexes of the Fe-only hydrogenase active site, $[\mathbf{1}{-}\mathbf{2H^N2H^{Fe}}]^{4+}$, that possesses both the NH proton and bridging Fe-hydride, and its precursor $[\mathbf{1}{-}\mathbf{2H^N}]^{2+}$ that possesses the NH proton. The protons coordinate to the aza nitrogen sites of **1** generate $[\mathbf{1}{-}\mathbf{2H^N}]^{2+}$ which further leads to $[\mathbf{1}{-}\mathbf{2H^N2H^{Fe}}]^{4+}$ with hydrides embedded within the Fe−Fe vectors while more protons are available. Such introduction of protons to the aza nitrogen site and the Fe−Fe bond, respectively, moves the reduction potential for about 1.2 V toward a more positive region. This result suggests that the ability to accept protons for the aza nitrogen and the Fe sites is essential for the enzymatic H_2 production at the mild potential.

Site-specific deprotonation of $[\mathbf{1}{-}\mathbf{2H^N2H^{Fe}}]^{4+}$ is facilitated by usage of different reagents. TEOA removes the NH protons of $[\mathbf{1}{-}\mathbf{2H^N2H^{Fe}}]^{4+}$ to generate the kinetic product, $[\mathbf{1}{-}\mathbf{2H^{Fe}}]^{2+}$, which converts to its thermodynamically stable tautomer, $[\mathbf{1}{-}\mathbf{2H^N}]^{2+}$. Deprotonation of the Fe hydride proceeds in the presence of chloride. The pK_a values

Table 1. X-ray Crystallographic Data of **1**, $[\mathbf{1-2H^N}]^{2+}$, and $[\mathbf{1-2H^N2H^{Fe}}]^{4+}$

	1	$[\mathbf{1-2H^N}](BF_4)_2\cdot 2CH_2Cl_2$	$[\mathbf{1-2H^N2H^{Fe}}](BF_4)_4\cdot 4CH_3CN$
empirical formula	$C_{34}H_{68}Fe_4N_2O_8P_4S_4$	$C_{36}H_{72}B_2Cl_4F_8Fe_4N_2O_8P_4S_4$	$C_{42}H_{82}B_4F_{16}Fe_4N_6O_8P_4S_4$
formula weight	1108.42	1451.90	1621.90
T, K	150(2)	150(2)	150(2)
crystal system	triclinic	orthorhombic	triclinic
space group	$P\bar{1}$	$Pna2_1$	$P\bar{1}$
a, Å	11.7164(9)	26.2091(17)	12.0713(5)
b, Å	14.0018(15)	11.9446(7)	12.7630(5)
c, Å	16.7238(17)	20.3932(13)	14.1186(5)
α, deg	112.986(9)	90	107.990(2)
β, deg	90.204(7)	90	94.040(2)
γ, deg	101.705(8)	90	113.709(2)
V, Å^3	2462.7(4)	6384.2(7)	1846.32(12)
Z	2	4	1
ρ_{calcd}, Mg m^{-3}	1.495	1.511	1.459
μ, mm^{-1}	1.499	1.355	1.056
F (000)	1156	2976	832
reflections collected	18111	47855	17715
independent reflections	18111	14451	6428
R_{int}	0.0000	0.0495	0.0326
Goodness-of-fit on F^2	1.060	1.154	1.018
R1 [$I > 2\sigma(I)$] (all data)[a]	0.0435 (0.0669)	0.0467 (0.0511)	0.1031 (0.1225)
wR2 [$I > 2\sigma(I)$] (all data)[b]	0.1040 (0.1181)	0.1116 (0.1159)	0.2985 (0.3227)

[a] $R1 = \sum||F_o| - |F_c||/\sum|F_o|$. [b] $wR2 = [\sum w(F_o^2 - F_c^2)^2/\sum w(F_o^2)^2]^{1/2}$.

of the aza nitrogen ($8.9 < pK_a^N < 15.9$) and the diiron sites ($pK_a^{FeFe} < 8.9$) are estimated from studies of protonation and deprotonation.

Four irreversible reduction events are recorded in the absence of a proton source for $[\mathbf{1-2H^N2H^{Fe}}]^{4+}$. According to bulk electrolysis and voltammetry in combination of titration experiments with acids, they are assigned to reduction of $[\mathbf{1-2H^N2H^{Fe}}]^{4+}$, $[\mathbf{1-2H^{Fe}}]^{2+}$, $[\mathbf{1-2H^N}]^{2+}$, and **1** from the ease of the working potential. Their presence in solution tentatively suggests that these four species probably are involved in the mechanism of electrocatalytic H_2 formation. Further studies to probe their roles in the catalytic mechanism are currently under investigation.

Experimental Section

General Methods. All reactions were carried out by using standard Schlenk and vacuum-line techniques under an atmosphere of purified nitrogen. All commercial available chemicals from Aldrich were of ACS grade and used without further purification. Solvents were of HPLC grade and purified as follows: Hexane, diethyl ether, and tetrahydrofuran (THF) were distilled from sodium/benzophenone under N_2. Dichloromethane was distilled from CaH_2 under N_2. Acetonitrile was distilled first over CaH_2 and then from P_2O_5 under N_2. Deuterated solvents obtained from Merck were distilled over 4 Å molecular sieves under N_2 prior to use. $^nPrN(CH_2CH_2SH)_2$ were prepared according to related literature procedures.[29]

Infrared spectra were recorded on a Perkin-Elmer Spectrum One using a 0.05 mm CaF_2 cell. ^1H, $^{13}C\{^1H\}$, and $^{31}P\{^1H\}$ NMR spectra were recorded on a Bruker AV-500 or DRX-500 spectrometer operating at 500, 125.7, and 202.49 MHz, respectively. Mass spectral analyses were done on a Waters LCT Premier XE at Mass Spectrometry Center in Institute of Chemistry, Academia Sinica. Elemental analyses were performed on an Elementar vario EL III elemental analyzer. Analysis of H_2 gas from bulk electrolysis was performed on an Agilent 6890 gas chromatograph with a TCD detector and a Supelco Carboxen 1000 column. Argon was used as the carrier gas.

Molecular Structure Determinations. The X-ray single crystal crystallographic data collections for **1**, $[\mathbf{1-2H^N}]^{2+}$, and $[\mathbf{1-2H^N2H^{Fe}}]^{4+}$ were carried out at 150 K on a Bruker SMART APEX CCD four-circle diffractometer with graphite-monochromated Mo Kα radiation (λ = 0.71073 Å) outfitted with a low-temperature, nitrogen-stream aperture. The structures were solved using direct methods, in conjunction with standard difference Fourier techniques, and refined by full-matrix least-squares procedures. A summary of the crystallographic data for complexes **1**, $[\mathbf{1-2H^N}]^{2+}$, and $[\mathbf{1-2H^N2H^{Fe}}]^{4+}$ is shown in Table 1. Selected metric data of **1**, $[\mathbf{1-2H^N}]^{2+}$, and $[\mathbf{1-2H^N2H^{Fe}}]^{4+}$ are listed in Table 2. An empirical absorption correction (multiscan) was applied to the diffraction data for all structures. All non-hydrogen atoms were refined anisotropically, and all hydrogen atoms were placed in geometrically calculated positions by the riding model. All software used for diffraction data processing and crystal structure solution and refinement are contained in the SHELXTL97 program suites.[30] The crystals of **1** suitable for X-ray analysis are in twin form. The crystallographic data are solved by twin refinement, and two molecules are presents in the unit cell. For $[\mathbf{1-2H^N}]^{2+}$, the methyl groups from one of the PMe_3 ligands, C(26), C(27), and C(28), are disordered. For $[\mathbf{1-2H^N2H^{Fe}}]^{4+}$, the fluorine atoms from one of the BF_4 anions, F(5), F(6), F(7), and F(8), exhibit disorder.

Electrochemistry. Electrochemical measurements were recorded on a CH Instruments 630C electrochemical potentiostat using a gastight three-electrode cell under N_2 at room temperature. A glassy carbon electrode (3 mm in diameter) and a platinum wire were used as working and auxiliary electrode, respectively. Reference electrode was a non-aqueous Ag/Ag^+ electrode (0.01 M $AgNO_3$/0.1 M n-Bu_4NPF_6). All potentials are measured in 0.1 M n-Bu_4NPF_6 solution in CH_3CN and reported against ferrocene/ferrocenium (Fc/Fc^+). Increments of acids were added by microsyringe.

Spectroelectrochemistry was performed by a Mettler Toledo ReactIR iC10 in situ FTIR system equipped with a MCT detector and a 0.625″ SiComp probe. Graphite rods (6.15 mm in diameter) were used as working and auxiliary electrodes. Reference electrode was a non-aqueous Ag/Ag^+ electrode

(29) (a) Karlin, K. D.; Lippard, S. J. *J. Am. Chem. Soc.* **1976**, *98*, 6951–6957. (b) Harley-Mason, J. *J. Chem. Soc.* **1947**, 320–322. (c) Snyder, H. R.; Stewart, J. M.; Ziegler, J. B. *J. Am. Chem. Soc.* **1947**, *69*, 2672–2674.

(30) *SHELXTL*, ver. 6.10; Bruker Analytical X-Ray Systems: Madison, WI, 2000.

Table 2. Selected Bond Lengths (Å) and Angles (deg) for **1**, $[\mathbf{1-2H^N}]^{2+}$, and $[\mathbf{1-2H^N2H^{Fe}}]^{4+}$

		1	
Fe(1)−Fe(2)	2.5433(6)	S(1)−Fe(1)−S(2)	81.18(3)
Fe(1)−S(1)	2.2737(8)	S(1)−Fe(1)−Fe(2)	55.96(2)
Fe(1)−S(2)	2.2528(8)	S(2)−Fe(1)−Fe(2)	55.82(2)
Fe(2)−S(1)	2.2724(8)	S(1)−Fe(2)−S(2)	81.06(3)
Fe(2)−S(2)	2.2597(8)	S(1)−Fe(2)−Fe(1)	56.01(2)
Fe(1)−P(1)	2.2000(9)	S(2)−Fe(2)−Fe(1)	55.57(2)
Fe(2)−P(2)	2.2110(9)	Fe(2)−S(1)−Fe(1)	68.03(3)
Fe−$C_{CO,ap}$	1.763(3)	Fe(2)−S(2)−Fe(1)	68.61(3)
Fe−$C_{CO,ba}$	1.757[b]		
		$[\mathbf{1-2H^N}]^{2+}$	
Fe(1)−Fe(2)	2.5641(8)	S(1)−Fe(1)−S(3)	80.97(4)
Fe(3)−Fe(4)	2.5348(8)	S(1)−Fe(1)−Fe(2)	55.43(3)
Fe(1)−S(1)	2.2517(11)	S(3)−Fe(1)−Fe(2)	55.27(3)
Fe(1)−S(3)	2.2485(12)	S(1)−Fe(2)−S(3)	80.84(4)
Fe(1)−P(1)	2.2277(13)	S(1)−Fe(2)−Fe(1)	55.24(3)
Fe(2)−S(1)	2.2567(11)	S(3)−Fe(2)−Fe(1)	55.23(3)
Fe(2)−S(3)	2.2496(11)	S(4)−Fe(3)−S(2)	81.21(4)
Fe(2)−P(2)	2.2127(13)	S(4)−Fe(3)−Fe(4)	56.22(3)
Fe(3)−S(2)	2.2619(11)	S(2)−Fe(3)−Fe(4)	56.51(3)
Fe(3)−S(4)	2.2707(11)	S(4)−Fe(4)−S(2)	80.63(4)
Fe(3)−P(3)	2.2088(12)	S(4)−Fe(4)−Fe(3)	56.01(3)
Fe(4)−S(2)	2.2836(11)	S(2)−Fe(4)−Fe(3)	55.70(3)
Fe(4)−S(4)	2.2763(12)	Fe(1)−S(1)−Fe(2)	69.33(3)
Fe(4)−P(4)	2.2208(13)	Fe(4)−S(2)−Fe(3)	67.79(3)
Fe−$C_{CO,ap}$	1.768[a]	Fe(2)−S(3)−Fe(1)	69.51(4)
Fe−$C_{CO,ba}$	1.762[b]	Fe(3)−S(4)−Fe(4)	67.76(4)
		$[\mathbf{1-2H^N2H^{Fe}}]^{4+}$	
Fe(1)−Fe(2)	2.5770(15)	S(2)−Fe(1)−S(1)	81.26(8)
Fe(1)−S(1)	2.281(2)	S(2)−Fe(1)−Fe(2)	55.32(7)
Fe(1)−S(2)	2.273(2)	S(1)−Fe(1)−Fe(2)	55.64(6)
Fe(1)−P(1)	2.236(2)	S(2)−Fe(2)−S(1)	81.35(8)
Fe(2)−S(1)	2.282(2)	S(2)−Fe(2)−Fe(1)	55.52(6)
Fe(2)−S(2)	2.268(3)	S(1)−Fe(2)−Fe(1)	55.59(6)
Fe(2)−P(2)	2.248(3)	Fe(2)−S(1)−Fe(1)	68.77(7)
Fe−$C_{CO,ap}$	1.786(9)	Fe(2)−S(2)−Fe(1)	69.16(7)
Fe−$C_{CO,ba}$	1.788[b]		

[a] Averaged values of d(Fe-CO_{ap}). [b] Averaged values of d(Fe-CO_{ba}).

(0.01 M $AgNO_3$/0.1 M n-Bu_4NPF_6), which was placed in a separated compartment with a fine porosity glass frit. The solution was stirred under N_2 throughout bulk electrolysis.

Synthesis of $[Fe_2(\mu\text{-}S(CH_2)_2N^nPr(CH_2)_2S)(CO)_6]_2$. A solution of $Fe_3(CO)_{12}$ (1.0 g, 1.98 mmol) in THF (20 mL) was treated with ^{n}PrN(CH_2CH_2SH)$_2$ (0.394 g, 2.2 mmol). The reaction mixture was then stirred at a refluxing temperature for 30 min. The resulting brown-red mixture was evaporated to dryness in vacuo, and the crude product was purified by chromatography on silica gel with CH_2Cl_2/hexane (v/v 1/1) as the eluent. From the red band, $[Fe_2(\mu\text{-}S(CH_2)_2N^nPr(CH_2)_2S)(CO)_6]_2$ (0.145 g, 16%) was obtained as a red solid. IR (hexane, cm^{-1}): ν_{CO} 2069 (m), 2037 (vs), 1999 (s), 1988 (s), 1973 (w), 1955 (vw). ^{1}H NMR (500 MHz, $CDCl_3$): 0.88 (t, $^3J_{CH}$ = 7.3 Hz, 6H, $CH_2CH_2CH_3$), 1.50 (sext, $^3J_{CH}$ = 7.5 Hz, 4H, $CH_2CH_2CH_3$), 2.34 (t, 4H, $CH_2CH_2CH_3$), 2.35 (t, 4H, SCH_2), 2.43 (t, 4H, NCH_2), 2.46 (t, 4H, SCH_2), 2.69 (t, 4H, NCH_2) ppm. ^{13}C{^{1}H} NMR (125.7 MHz, $CDCl_3$): 11.68 ($CH_2CH_2CH_3$), 20.36 ($CH_2CH_2CH_3$), 23.65 (SCH_2), 38.13 (SCH_2), 55.08 (NCH_2), 56.02 (NCH_2), 57.03 ($CH_2CH_2CH_3$), 208.87 (CO) ppm. ESI-MS: m/z 914.8 $\{M + H^+\}^+$. Anal. Calcd for $C_{26}H_{30}Fe_4N_2O_{12}S_4$: C, 34.16; H, 3.31; N, 3.06; S, 14.03. Found: C, 34.16; H, 3.34; N, 3.00; S, 14.05.

Synthesis of $[Fe_2(\mu\text{-}S(CH_2)_2N^nPr(CH_2)_2S)(CO)_4(PMe_3)_2]_2$, 1. To a solution of $[Fe_2(\mu\text{-}S(CH_2)_2N^nPr(CH_2)_2S)(CO)_6]_2$ (500 mg, 0.55 mmol) in THF (10 mL) was added PMe_3 (2.74 μL, 2.75 mmol, 1 M in THF) via an airtight microsyringe. The reaction solution was stirred at room temperature for 2 h before it was dried in vacuo. The solid was washed three times with 10 mL portions of hexane. A red powder was obtained in 85% yield. Crystals of **1** suitable for X-ray crystallographic analysis were grown from a CH_2Cl_2 solution layered with hexane. IR (CH_2Cl_2, cm^{-1}): ν_{CO} 1975 (s), 1939 (vs), 1905 (s), 1887 (m). ^{1}H NMR (500 MHz, CD_2Cl_2): 0.83 (t, 6H, CH_3), 1.39 (hex, 4H, $CH_3CH_2CH_2$), 1.53 (d, $^2J_{HP}$ = 9 Hz, 36H, PMe_3), 2.10 (br, 4H, SCH_2), 2.33 (t, 8H, SCH_2, $CH_3CH_2CH_2$), 2.49 (t, 4H, NCH_2), 2.68 (t, 4H, NCH_2) ppm. ^{31}P NMR (202.49 MHz, CD_2Cl_2): 20.34 (br) ppm. ESI-MS: m/z 1106.99 $\{\mathbf{1} + H^+\}^+$, 554.00 $\{\mathbf{1} + 2H^+\}^{2+}$. Anal. Calcd for $C_{34}H_{66}Fe_4N_2O_8P_4S_4$: C, 36.91; H, 6.01; N, 2.53, S, 11.59. Found: C, 36.84; H, 5.97; N, 2.51, S, 11.67. CV (THF, V vs Fc/Fc^+): −2.43 (E_{pc}).

Synthesis of $[Fe_2(\mu\text{-}S(CH_2)_2N^nPr(H)(CH_2)_2S)(CO)_4(PMe_3)_2]_2$-$(BF_4)_2$, $[\mathbf{1-2H^N}](BF_4)_2$. To a solution of **1** (300 mg, 0.27 mmol) in CH_2Cl_2 (10 mL) was added HBF_4 (68.4 μL, 0.54 mmol, 50 wt % in H_2O) via an airtight microsyringe. The reaction mixture was stirred at room temperature for 30 min and monitored by FTIR spectroscopy. After the reaction was finished, it was dried in vacuo. The solid residue was washed twice with 10 mL portions of ether. A red powder was obtained in almost quantitative yield. Crystals of $[\mathbf{1-2H^N}](BF_4)_2\cdot 2CH_2Cl_2$ suitable for X-ray crystallographic analysis were grown from a CH_2Cl_2 solution layered with ether. IR (CH_2Cl_2, cm^{-1}): ν_{CO} 1987 (s), 1948 (vs), 1920 (s), 1891 (m). ^{1}H NMR (500 MHz, CD_2Cl_2): 1.03 (t, 6H, CH_3), 1.50 (d, $^2J_{HP}$ = 9.5 Hz, 18H, PMe_3), 1.64 (d, $^2J_{HP}$ = 9 Hz, 18H, PMe_3), 1.80 (m, 4H, $CH_3CH_2CH_2$), 2.11−2.64 (m, 8H, SCH_2), 2.94−3.78 (m, 12H, NCH_2), 7.42 (br, 2H, NH) ppm. ^{31}P NMR (202.49 MHz, CD_2Cl_2): 10.71 (d, J_{PP} = 9.9 Hz), 29.43 (d, J_{PP} = 9.5 Hz) ppm. ESI-MS: m/z 1195.04 $\{[\mathbf{1-2H^N}](BF_4)\}^+$, 1107.03 $\{[\mathbf{1-2H^N}] - H^+\}^+$, 554.01 $\{[\mathbf{1-2H^N}]\}^{2+}$. Anal. Calcd for $C_{36}H_{72}B_2Cl_4F_8Fe_4N_2O_8P_4S_4$: C, 31.85; H, 5.35; N, 2.19. Found: C, 31.33; H, 5.46; N, 2.18. CV (CH_3CN, V vs Fc/Fc^+): −1.82 and −2.43 (E_{pc}), +0.01 (E_{pa}).

Synthesis of $[Fe_2(\mu\text{-}H)(\mu\text{-}S(CH_2)_2N^nPr(H)(CH_2)_2S)(CO)_4$-$(PMe_3)_2]_2(BF_4)_4$, $[\mathbf{1-2H^N2H^{Fe}}](BF_4)_4$. Method A. To a solution of **1** (300 mg, 0.27 mmol) in CH_3CN (7 mL) was added HBF_4 (854.4 μL, 6.75 mmol, 50 wt % in H_2O) via an airtight microsyringe. The reaction mixture was stirred at room temperature for at least 1.5 h until FTIR indicated no more of the starting material was left. After the reaction was finished, it was dried in vacuo. The semi-solid residue was washed twice with 15 mL portions of ether first and then CH_3CN/ether solution until the powder was obtained. The yield was 85%.

Method B. To a solution of $[\mathbf{1-2H^N}](BF_4)_2$ (221 mg, 0.2 mmol) in CH_3CN (7 mL) was added HBF_4 (630 μL, 5 mmol, 50 wt % in H_2O) via an airtight microsyringe. The solution was stirred at room temperature for 1 h before it was dried under vacuum. The semi-oil residue was washed three times with 20 mL portions of ether. The powder product was obtained after the second wash with CH_3CN/ether. The yield was 87%. Crystals of $[\mathbf{1-2H^N2H^{Fe}}](BF_4)_4\cdot 4CH_3CN$ suitable for X-ray crystallographic analysis were grown from a mixed CH_3CN/CH_2Cl_2 solution layered with ether. IR (CH_3CN, cm^{-1}): ν_{CO} 2058 (s), 2039 (vs), 2006 (s), 1993 (s, sh). ^{1}H NMR (500 MHz, CD_2Cl_2): −15.46 (d, $^2J_{HP}$ = 21.5 Hz, 2H, FeHFe), 0.96 (t, 6H, CH_3), 1.74 (d, $^2J_{HP}$ = 10.5 Hz, 18H, PMe_3), 1.97 (d, $^2J_{HP}$ = 11 Hz, 18H, PMe_3), 1.70−2.01 (m, 4H, $CH_3CH_2CH_2$), 2.24−2.92 (m, 8H, SCH_2), 3.23−3.74 (m, 12H, NCH_2), 9.08 (br, 2H, NH) ppm. ^{31}P NMR (202.49 MHz, CD_2Cl_2): 19.58 (d, J_{PP} = 7.89 Hz), 23.43 (dd, J_{PP} = 7.69 Hz) ppm. ESI-MS: m/z 1371.06 $\{[\mathbf{1-2H^N2H^{Fe}}](BF_4)_3\}^+$, 1283.04 $\{[\mathbf{1-2H^N2H^{Fe}}](BF_4)_2 - H^+\}^+$, 1195.02 $\{[\mathbf{1-2H^N2H^{Fe}}]$-$(BF_4) - 2H^+\}^+$, 1106.8 $\{[\mathbf{1-2H^N2H^{Fe}}] - 3H^+\}^+$, 598.02 $\{[\mathbf{1-2H^N2H^{Fe}}](BF_4) - H^+\}^{2+}$, 554.1 $\{[\mathbf{1-2H^N2H^{Fe}}] - 2H^+\}^{2+}$. Anal. Calcd for $C_{42}H_{82}B_4F_{16}Fe_4N_6O_8P_4S_4$: C, 31.10; H, 5.10; N, 5.18. Found: C, 31.32; H, 5.12; N, 5.15. CV (CH_3CN, V vs Fc/Fc^+): −1.26, −1.42, −1.82, and −2.43 (E_{pc}).

Reaction of $[\mathbf{1-2H^N2H^{Fe}}](BF_4)_4$ with Triethanolamine (TEOA). To a 5 mL CH_3CN solution of $[\mathbf{1-2H^N2H^{Fe}}](BF_4)_4$

(97 mg, 0.067 mmol) was added 2 equiv of TEOA (17.7 μL, 0.133 mmol) by microsyringe. The reaction was monitored by IR spectroscopy, indicating that the IR bands of $[\mathbf{1-2H^N2H^{Fe}}](BF_4)_4$ were red-shifted about 10 cm^{-1} within 10 min. The product was assigned to $[\mathbf{1-2H^{Fe}}](BF_4)_2$. Attempt to isolate the pure sample of $[\mathbf{1-2H^{Fe}}]^{2+}$ failed because of its instability in solution. $[\mathbf{1-2H^{Fe}}]^{2+}$ converted to $[\mathbf{1-2H^N}]^{2+}$ in solution, evidenced by IR spectroscopy. $[\mathbf{1-2H^N}]^{2+}$ was the final product if $[\mathbf{1-2H^{Fe}}]^{2+}$ was left in solution overnight, confirmed by NMR and FTIR analyses. When excess TEOA (5 equiv) was initially added to the solution instead, both of $[\mathbf{1-2H^{Fe}}]^{2+}$ and **1** were observed immediately in the IR spectrum. IR changes of the reaction revealed that intensity of the IR bands from **1** increased as that of $[\mathbf{1-2H^{Fe}}]^{2+}$ decreased. Complex **1** eventually was the sole product according to IR and NMR characterization. $[\mathbf{1-2H^{Fe}}]^{2+}$: IR ($CH_3CN$, cm^{-1}): ν_{CO} 2049 (m), 2032 (vs), 1993 (s).

Reaction of $[\mathbf{1-2H^N2H^{Fe}}](BF_4)_4$ with [PPN]Cl. To a 10 mL CH_3CN solution of $[\mathbf{1-2H^N2H^{Fe}}](BF_4)_4$ (100 mg, 0.069 mmol) was added 8 equiv of [PPN]Cl (317 mg, 0.552 mmol). The reaction was monitored by IR spectroscopy. A new set of ν(CO) bands at 1982, 1945, 1914, and 1892 cm^{-1} was observed within 4 min, indicating formation of $[\mathbf{1-2H^N}](BF_4)_2$. The solution was dried under vacuum and washed by CH_2Cl_2/hexane. Characterization of the solid to be $[\mathbf{1-2H^N}]^{2+}$ was confirmed by NMR and MS analyses. $[\mathbf{1-2H^N}]^{2+}$: IR (CH_3CN, cm^{-1}): ν_{CO} 1982 (s), 1945 (vs), 1914 (s), 1892 (m).

Acknowledgment. We are grateful to financial support from National Science Council of Taiwan and Academia Sinica. We thank Prof. Wen-Feng Liaw (National Tsing Hua University) for insightful discussions. We also thank Drs. Mei-Chun Tseng and Su-Ching Lin for help with MS analysis and 2D NMR experiments, respectively.

Supporting Information Available: Crystallographic data of **1**, $[\mathbf{1-2H^N}]^{2+}$, and $[\mathbf{1-2H^N2H^{Fe}}]^{4+}$ in CIF format. This material is available free of charge via the Internet at http://pubs.acs.org.